Journal of the European Ceramic Society **16** (1996) 217–224

0955-2219(95)00133-6
0955-2219/96/$15.00

Mechanical Properties of Mullite Materials

M. I. Osendi & C. Baudín

Instituto de Cerámica y Vidrio (CSIC), E-28500, Arganda del Rey, Madrid, Spain

(Accepted 22 July 1995)

Abstract

The mechanical behaviour of two $3Al_2O_3{\cdot}2SiO_2$ dense mullite materials with the same level of impurities but different in nature has been studied. Microstructure has been characterized by SEM and TEM. Toughness, bend strength and Young's modulus have been determined from room temperature up to 1400°C. Dependence of toughness on strain rate has been investigated. Special attention has been paid to correlate the trend of the mechanical parameters to fractographic observations by SEM.

1 Introduction

Nowadays, highly reactive, homogeneous and pure mullite powders that allow us to obtain high density structural $3Al_2O_3{\cdot}2SiO_2$ mullite materials are available.[1] In these materials, the mullite phase is the 3:2 one. Even though the starting powders are highly pure, small amounts of impurities, whose nature depends on the synthesis route,[2] are always present. When powders are obtained by sol–gel methods the main contaminants come from the milling media, (eg. ZrO_2), whilst when mullite powders are fabricated from raw materials, the main impurities are alkalis and alkaline–earths. Some impurities, like iron oxide and titania,[3] can enter in solid solution in mullite in rather large quantities or, like zirconia, remain mostly as isolated particles[4] while others, like alkaline oxides can form liquids at rather low temperatures, (eg. T ~1000°C for Na_2O).[5] After sintering of the mullite materials, a certain amount of liquid remains as glassy phases. Softening temperature and viscosity of these residual amorphous phases dramatically depend on their composition.[6,7] Moreover, quantity and distribution of these glassy phases in the material should depend on sintering temperature, and content and nature of the impurities.

From a mechanical point of view, the most studied property of mullite materials at high temperature has been creep.[8–12] A variety of mechanisms, from solid-state diffusion to viscous flow, and activation energies, ranging from 500 KJ/mol[8,9] to 1300 KJ/mol,[10] have been reported for mullite creep. This diversity in the data, in spite of the similar ranges of test temperatures and loads, could be attributed to slight differences in the impurity contents and their nature. In fact, small amounts of additives greatly change not only the viscosity of liquids[6] but, certainly, their wetting characteristics. Distribution of remaining glassy phases, along grain boundaries or forming isolated pockets, will influence creep mechanisms at high temperatures.

On the other hand, probably due to its inherent brittleness, fracture properties of mullite have been analyzed less.[13,14] In fact, most of the work has been devoted to establishing the relationships between mullite stoichiometry and parameters such as toughness and modulus of rupture.[15–20]

In the present work, the mechanical behaviour of two mullite materials with the same level of impurities but different in nature has been studied. The selected parameters have been toughness, bend strength, and Young's modulus. Variations of these parameters with temperature and strain rate have been obtained. Special attention has been paid to correlate the parameter trends to the aspect of the fracture surfaces.

2 Experimental

Two kinds of mullite materials henceforth labelled as MS0 and MB0 have been prepared from commercial powders* as previously described.[4] MS0 was processed from a commercial gel type mullite (1·5 μm of average particle size), that was spray dried, isostatically pressed and sintered at 1660°C for 2 h. MB0 powders were coarse grain commercial mullite, that were attrition milled with mullite balls down to 0·8 μm, before isostatically pressing and sintering at 1630°C for 4 h. Fundamental

*MS0: Chichibu Cement Co., supplied by Scimareck Ltd. Tokyo, Japan.
MB0: Baikowski Chimie, France.

Table 1. Main characteristics of the mullite materials

Material	*Dynamic Young's Modulus (GPa)*	*Density (g/cm^3)*	*Average grain size (μm)*	*Al_2O_3/SiO_2 ratio (wt%)*
MS0	202 ± 2	3·05 ± 0·02	1·2 ± 0·9	2·66
MB0	195 ± 4	3·01 ± 0·02	0·7 ± 0·5	2·75

Table 2. Impurity contents in the mullite materials

Material	*$Fe_2O_3 + TiO_2 + Y_2O_3$ (wt%)*	*$Na_2O + CaO + MgO + K_2O$ (wt%)*	*ZrO_2 (wt%)*
MS0	0·17	0·13	0·33
MB0	0·11	0·30	0·02

characteristics of the materials are collected in Table 1. Main impurities of these mullites are shown in Table 2.

Although the total level of impurities in both mullites is similar (< 0·65 wt% in MS0 and < 0·45 wt% in MB0) chemical compositions are quite different. The main impurity in MS0 is ZrO_2, followed far behind by TiO_2. Conversely, the more abundant impurities in MB0 are Na_2O and Fe_2O_3. The large amount of ZrO_2, found in MS0, is attributable to the powder milling procedure of the supplier.

Figure 1 shows representative microstructures (SEM) of the studied mullite materials. In MS0 some exaggerated grain growth and pore trapping have taken place whereas MB0 has a more uniform microstructure and mainly intergranular porosity.

In Fig. 2 the main characteristics of grain boundaries in MS0 samples are observed (TEM). Zirconia remains as particles (≈200 nm) located at triple points (Fig. 2(a)) while glassy pockets at grain junctions are scarcely observed (Fig. 2(b)). Figure 3 shows glassy pockets at triple points that are often present in MB0, where alkaline impurities concentrated as EDX analysis revealed. At the level of resolution employed no glassy phase films were observed along grain boundaries in any sample.

All mechanical and elastic tests were performed in an universal load testing machine with an electrically heated furnace, using 4-point bending fixtures made of SiC or Al_2O_3, with inner and outer spans of 20 and 40 mm.

Bend strength test measurements at temperatures ranging from RT to 1400°C were performed on 4 × 3 × 50 mm bars that were diamond machined from the sintered compacts, polished and chamfered on the tension surface. At least 5 bars were tested at each temperature.

Static Young's modulus (RT–1400°C) was calculated from the central point deflection of bend bars measured using a SiC probe attached to a LVDT through an alumina tube. Three bars were tested at each temperature. For bend strength and Young's modulus measurements, load was applied at 1000 N/min.

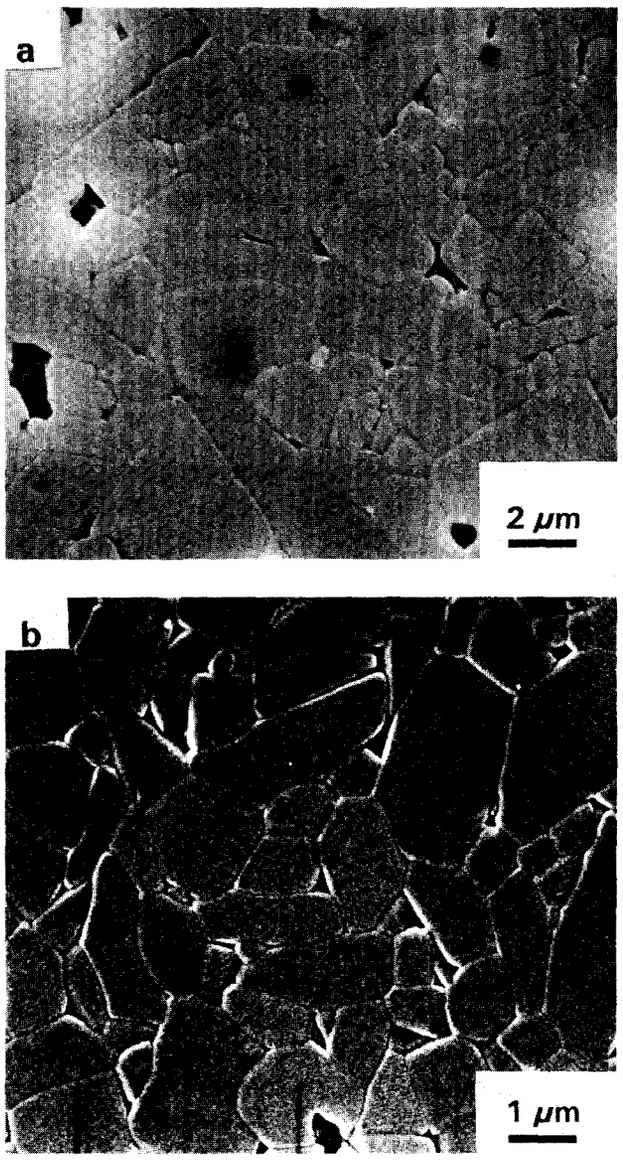

Fig. 1. Representative SEM microstructures of the studied mullite materials: (a) MS0; (b) MB0.

Toughness was determined by the SENB method using five bars for each temperature. Bars of dimension 4 × 6 × 50 mm were machined and

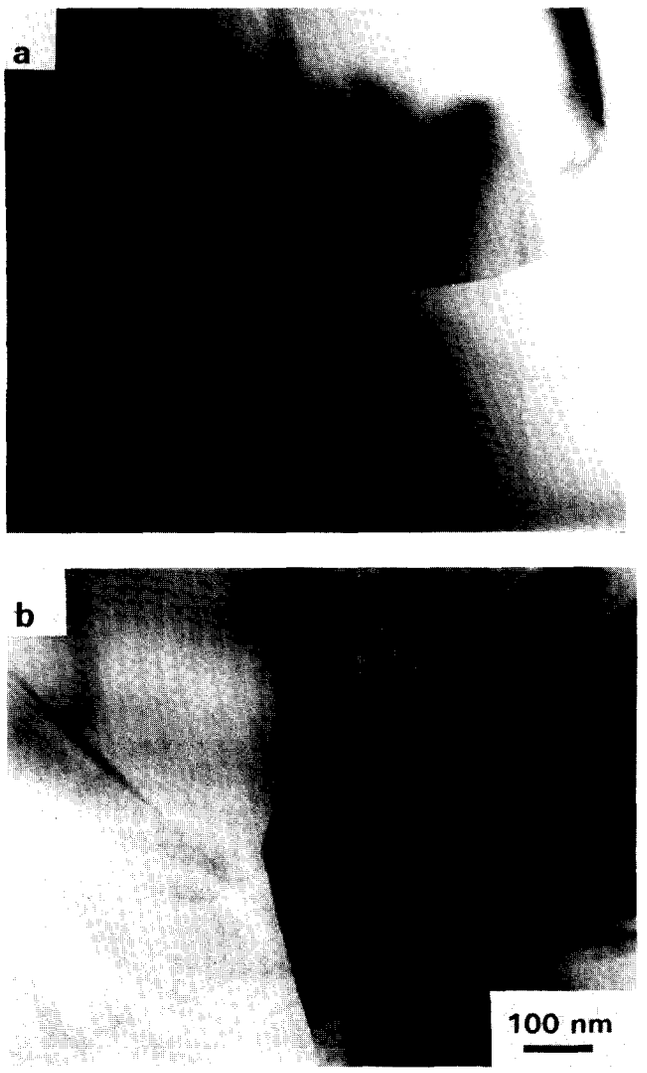

Fig. 2. TEM microstructures of MS0. The main characteristics of the grain boundaries are observed: (a) Zirconia located at triple points; (b) glassy pockets at grain junctions.

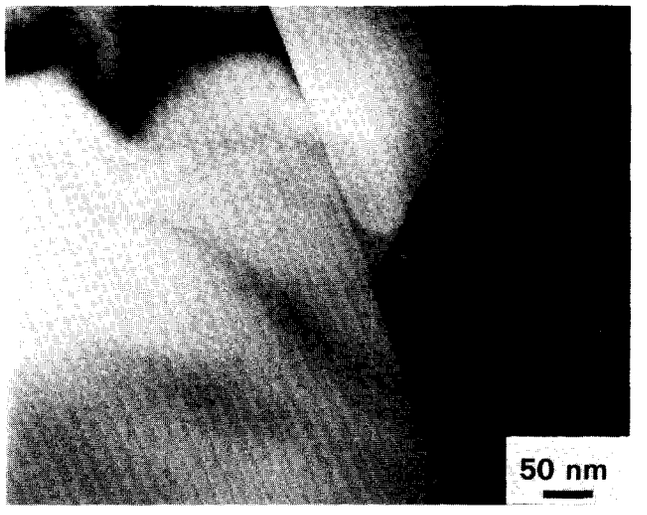

Fig. 3. TEM microstructure of MB0. Glassy pockets at triple points are observed.

notches were introduced with a thin diamond disc. Notches were 3 mm long and 200 μm width. The actuator rates ranged from 0·005 to 5 mm/min.

Polished and thermally etched (1500°C) samples and 'as fractured' surfaces were observed by SEM. Specimens were thinned, dimpled and Ar milled in order to be analyzed by TEM.

3 Results

In Fig. 4 static Young's modulus versus temperature is depicted. Room temperature values are the same for both materials and a slight decrease with temperature is observed.

Bend strength as a function of temperature is shown in Fig. 5. Values are always lower for MS0 although data trends are the same for both mullites, showing peaks in strength at T = 1200–1300°C.

Toughness values obtained using an actuator speed of 0·05 mm/min are represented in Fig. 6. Room temperature values are almost the same for

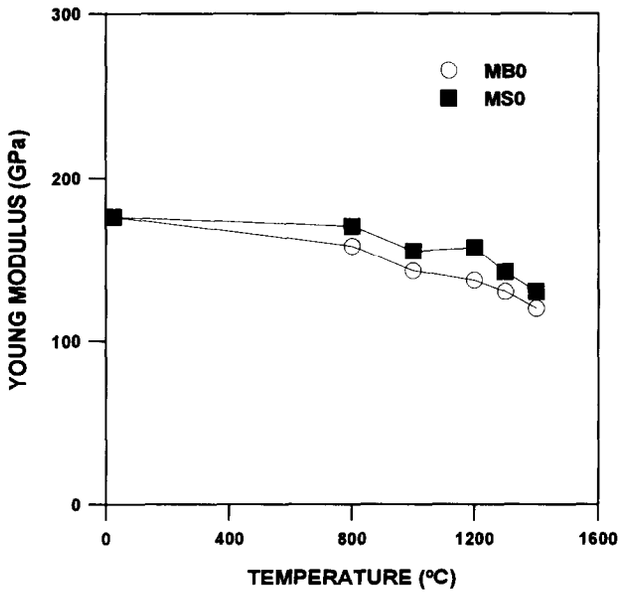

Fig. 4. Static Young's modulus versus temperature.

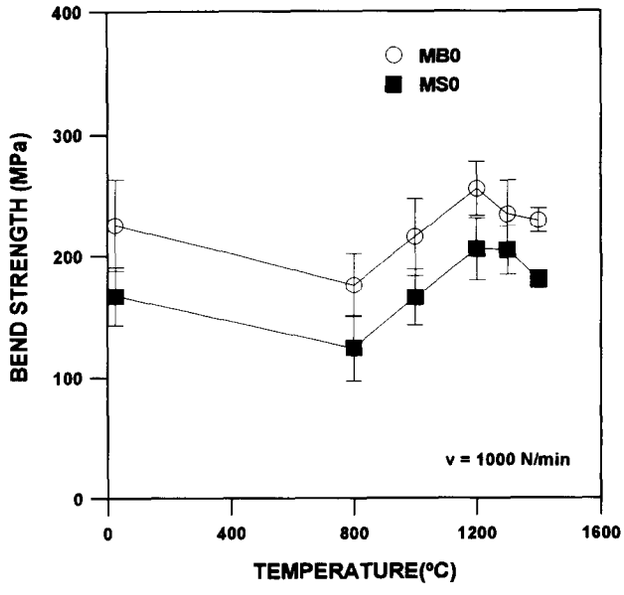

Fig. 5. Bend strength versus temperature.

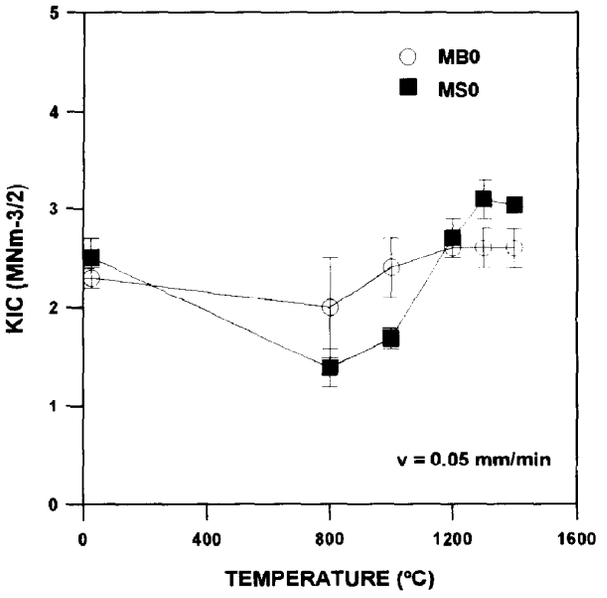

Fig. 6. Toughness values versus temperature obtained using an actuator speed of 0·05 mm/min.

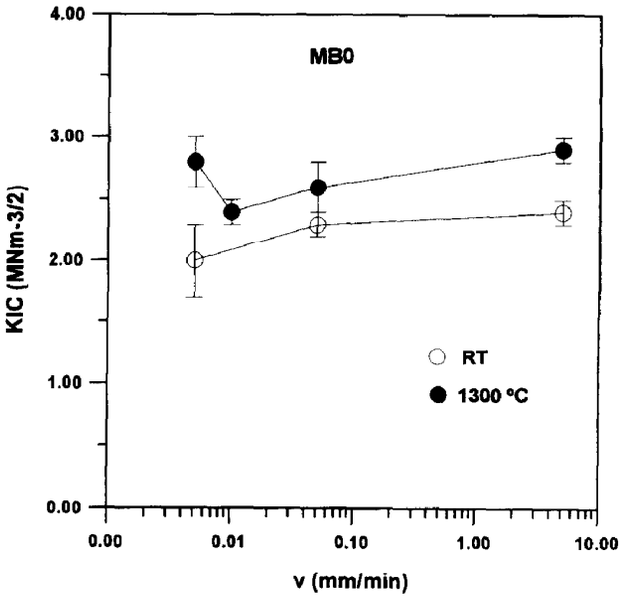

Fig. 8. K_{IC} data at room temperature and 1300°C as a function of the actuator speed for MB0.

both materials although toughness dependence on temperature is more marked for MS0, showing a decrease from room temperature up to 800 followed by a sudden increase.

Figures 7 and 8 show K_{IC} data as a function of the actuator speed tor MS0 and MB0. Tests were performed at room temperature and 1300°C. At room temperature, K_{IC} increases with strain rate for MS0 whereas K_{IC} is practically constant for MB0. At 1300°C, toughness values diminish as strain rate increases for MS0. The dependence of toughness on strain rate is not monotonous for MB0: maximum values are obtained using the slowest strain rate (0·005 mm/min) and a minimum is found for a strain rate of 0·01 m/min.

In Fig. 9 room temperature fracture surfaces of

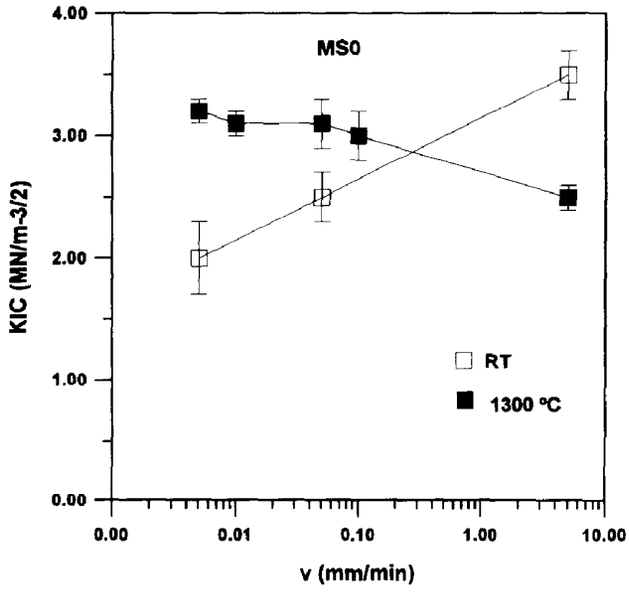

Fig. 7. K_{IC} data at room temperature and 1300°C as a function of the actuator speed for MS0.

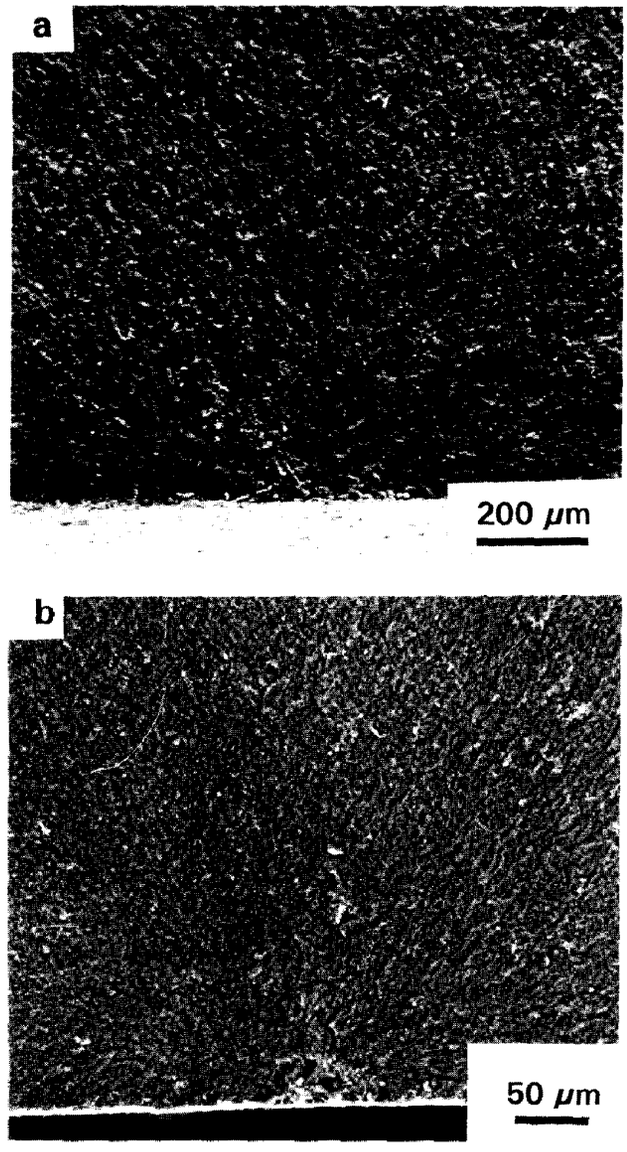

Fig. 9. Room temperature fracture surfaces of bend bars (SEM): (a) MS0; (b) MB0.

bend strength bars are displayed. In MS0, fracture origins are not well defined, but a characteristic semielliptical feature (diameter ≈150 μm) close to the tension surface is usually detected (Fig. 9(a)). Most of fracture origins in MB0 samples are pores (diameter ≈30 μm) as the one in Fig. 9(b).

Figure 10 shows typical fracture surfaces of MS0 notched bars after toughness testing. At room temperature, as well as at 1300°C, differentiated zones close to the notch exist (Fig. 10(a, b)). The size of these zones increased as strain rate decreased and as temperature increased. Higher magnification (Fig. 10(c)) shows that intergranular fracture predominates in these zones for tests done at room temperature. In parallel, in the samples tested at 1300°C the main features of the zone close to the notch are large areas ($d \approx 200$ μm for the slowest strain rate) at both surfaces of the crack that have crept, sliding one against the other, coexisting with intergranular fracture (Fig. 10(d)).

Fracture surfaces of MB0 toughness specimens are collected in Fig. 11. No special features are observed in the room temperature samples, being the fracture mainly transgranular through the whole specimen (Fig. 11(a, c)). Conversely, at 1300°C a differentiated zone close to the notch exist (Fig. 11(b)). Higher magnification (Fig. 11(d)) reveals a sharp transition from intergranular to transgranular fracture at the boundary of this zone. The size of this zone varies with loading rate and is minimum for samples tested at 0·005 mm/min.

4 Discussion

4.1 Room temperature mechanical behaviour

In order to explain the difference in the room temperature bend strength values, lower for MS0, whereas toughness values are about the same for both materials (Figs 5 and 6) the following equation should be considered:

$$\sigma_f = \frac{Z}{Y} \frac{K_{IC}}{\sqrt{c}}$$

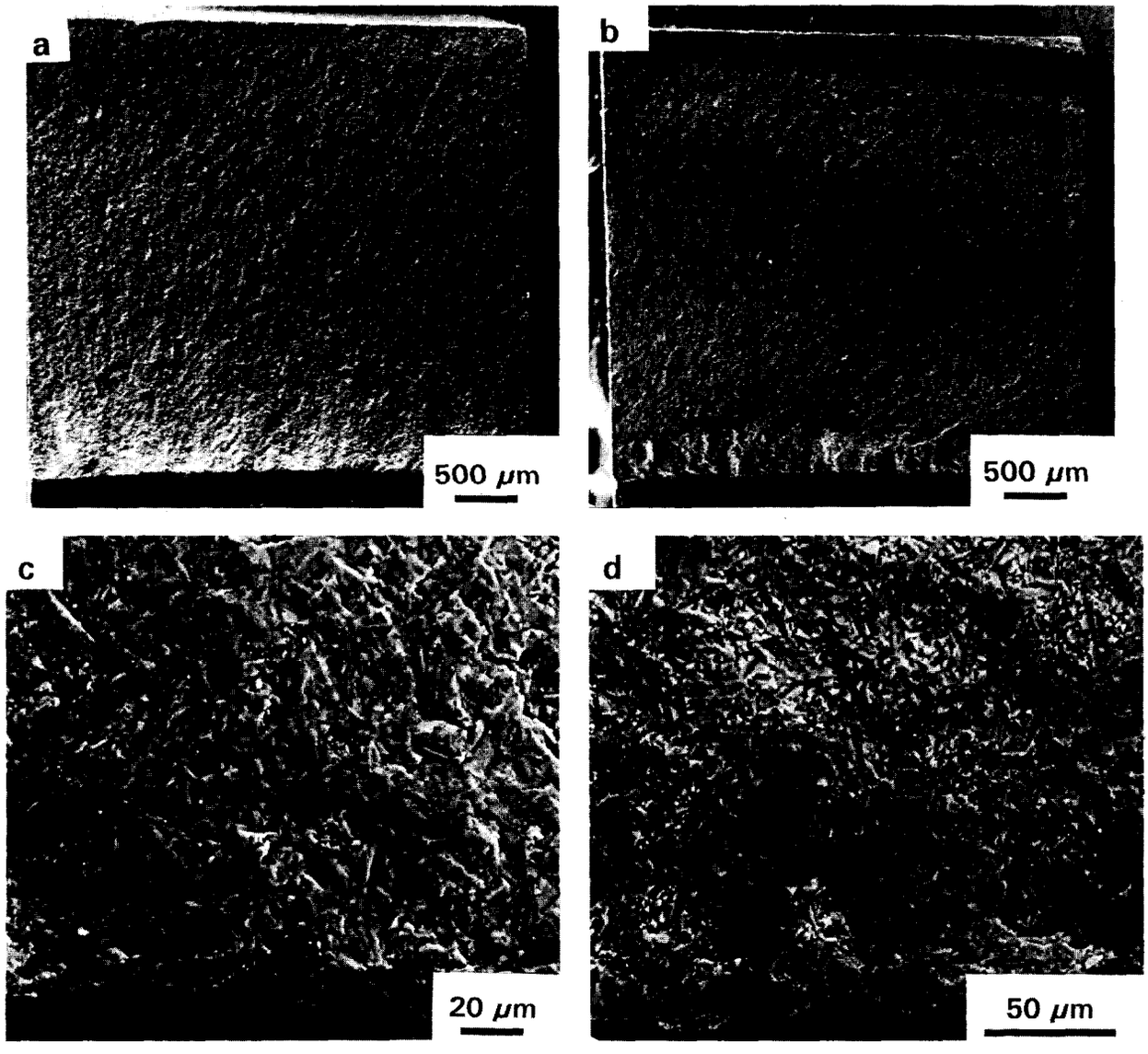

Fig. 10. Fracture surfaces of MS0 notched bars after toughness testing: (a) and (c) room temperature; (b) and (d) 1300°C.

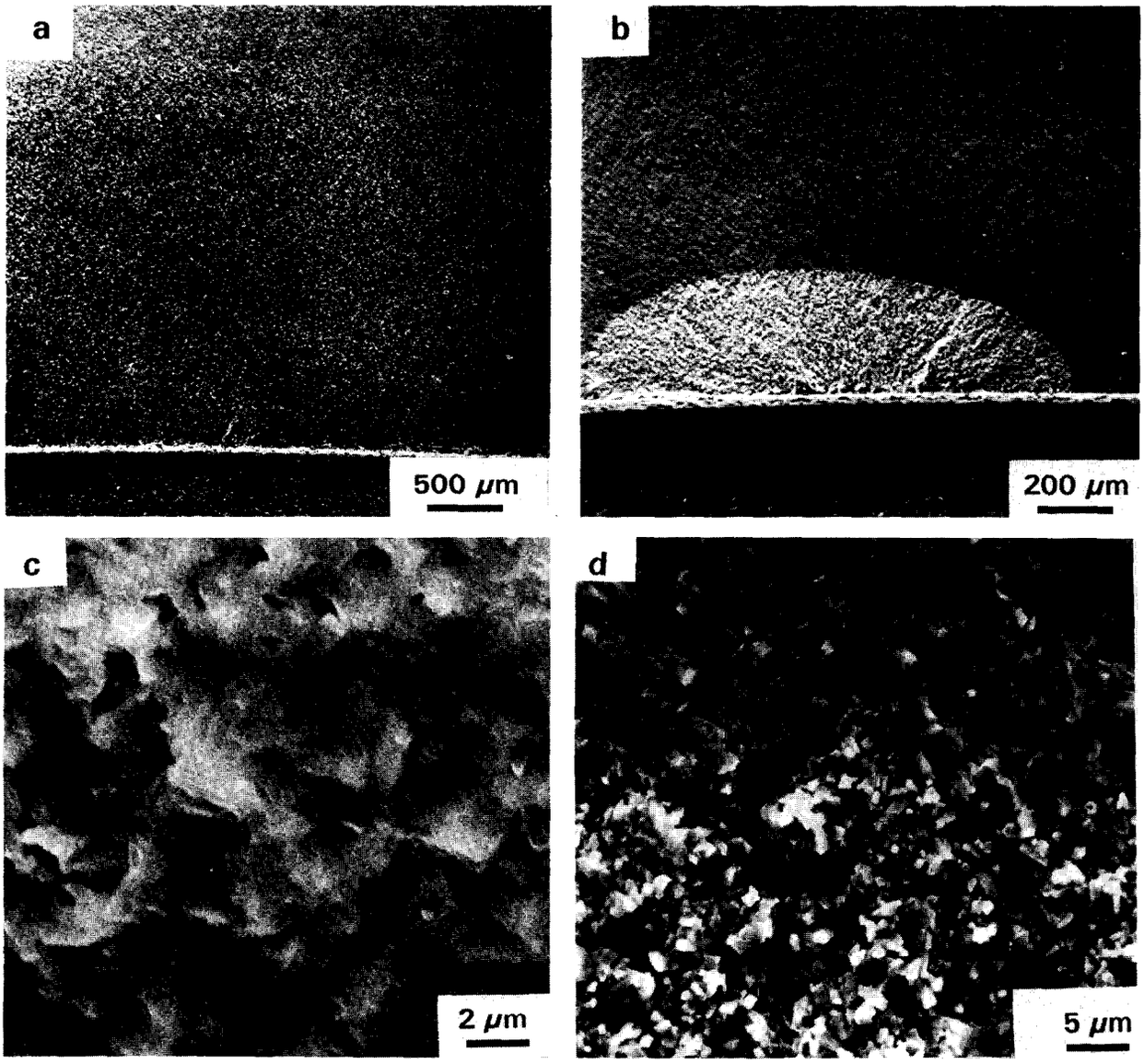

Fig. 11. Fracture surfaces of MB0 notched bars after toughness testing: (a) and (c) room temperature; (b) and (d) 1300°C.

Substituting the constant values for a semielliptical ($Z = 1{\cdot}6$) surface ($Y = 2$) crack of radius c[21] and introducing K_{IC} and σ_f limiting values into the expression, critical defect sizes ranging from 100 to 276 μm for MS0 and from 40 to 112 μm for MB0 are obtained.

In the case of MS0 specimens, these calculated critical flaw sizes agree well with the sizes of the semielliptical features observed close to the tension surfaces, as shown in Fig. 10(a). These semielliptical zones seem to develop from smaller processing defects by subcritical crack growth. Subcritical crack growth zones, defined by intergranular fracture mode, were also apparent on fracture surfaces of K_{IC} specimens tested at room temperature, as shown in Fig. 11(a,c). Moreover, toughness values determined using the slowest rate are much lower than those obtained at the fastest rate (Fig. 7). This trend of K_{IC} with loading rate also support subcritical crack growth in MS0.

Observing the fracture surfaces of MB0 specimens (Fig. 9(b)) fracture origin dimensions agree with the previous calculations. In fact, no dependence of room temperature K_{IC} values on loading rate occurs (Fig. 8) and no subcritical crack growth zone is observed close to the notch in toughness specimens (Fig. 11(a, c)). It is interesting to note that the range of loading rates that have been used is very large, thus apparently, no easy paths for crack growth exist in MB0.

The existence of subcritical crack growth at room temperature in MS0 and not in MB0 implies that grain boundaries are weaker in MS0 than in MB0. As mentioned in Section 2, no glassy films along grain boundaries were observed with the available techniques in neither mullite. Nevertheless, its presence in MS0 sample can be assumed considering the level of impurities and sintering temperatures. Furthermore, thin glassy films of $\approx$ 10 nm have been observed by other authors at

the mullite–mullite interfaces by HRTEM in the eutectic systems ZrO_2-mullite[22] and also in mullite materials doped with small amounts of ZrO_2.[23] These facts support the evidence that the glassy phase is preferentially located along grain boundaries in MS0, in agreement with TEM observations in which triple point glassy pockets were scarcely observed in MS0. Conversely, large amounts of glassy pockets were observed in MB0 comparatively to MS0, which suggests that glassy phase is preferentially located at triple points in agreement to the lack of subcritical crack growth at room temperature in MB0 mullite.

4.2 Mechanical behaviour up to 1400°C

The decrease in Young's moduli with temperature for both mullites (Fig. 4) is the expected one considering the rather high loading rate used. At this rate, materials remain linear elastic through the load cycle at each testing temperature.

In terms of bend strength, both mullites present the usual behaviour of ceramic materials with small glassy phase amounts (Fig. 5). The initial decrease is related to elastic bond relaxation as temperature increases as discussed above. The increase at temperatures higher than 1000°C can be associated to the softening of the residual glassy phases in the range of testing temperatures, which could lead to healing of the critical flaws or an increase in apparent toughness.

For each mullite, toughness and bend strength dependences on temperature (Figs 5 and 6) show only slight differences that can be attributed to differences in strain rates between both tests. Both mullites experience K_{IC} and σ_f peak values in the interval 1200–1300°C. Therefore, the increase in bend strengths at high temperature can easily be associated to the toughness behaviour.

Most ceramics, like the mullites studied here, contain remaining glassy phases that have been formed during sintering. In materials such as alumina, silicon nitride and glass ceramics,[24,25] peaks in strength and toughness with temperature have been associated with several phenomena derived from the softening of those remaining glassy phases.[26,27] A variety of mechanisms, from blunting of critical flaws to grain boundary sliding, crack branching or formation of crack bridges by viscous flow during crack propagation have been proposed.[22] Probably, not a single mechanism takes place but an interaction of several ones occurs depending on composition and distribution of the glass, testing temperature and strain rate.

In order to discern which of those mechanisms are predominant in the present mullite materials, K_{IC} data as a function of strain rate at two limiting temperatures RT and 1300°C were analyzed.

Considering first the MS0 samples, the increase in K_{IC} with strain rate at room temperature (Fig. 7) is due to subcritical crack growth through the easy paths provided by the glass phase as above discussed. The toughness behaviour at 1300°C is also attributed to the glassy phase, but the mechanism seems to be quite different. Actually, viscous flow at slow strain rates favors sliding between grains or agglomerates as can be observed on the micrographs of fracture surfaces at 1300°C (Fig. 10(b, d)). This grain boundary sliding phenomenon, and its related plastic deformation effect, produce higher apparent K_{IC} at slow strain rates, while at the very high strain rate it does not take place. Due to the lack of energy dissipative mechanisms at high strain rates, toughness values at high temperature are lower than at room temperature because of the decrease of the elastic modulus (Fig. 4), as experimentally observed in Fig. 7.

For MB0, K_{IC} values at 1300°C are always larger than at room temperature for each strain rate (Fig. 8) but, the energy absorbing mechanisms in this mullite are more complex than in MS0. In fact, the trend of K_{IC} values for MB0 samples with strain rate (Fig. 8) is opposite to that shown by MS0 and there is one point that does not follow the general trend (v = 0·005 mm/min). The K_{IC} fracture surfaces of MB0 samples (Fig. 1(b, d)) show process zones close to the notch, in which a total decohesion of the mullite grains is evident. This microstructural aspect could be due to migration of the low viscosity liquid phase during loading. The energy absorbing mechanisms associated to the liquid phase occur in MB0 through the whole range of strain rates, even at the very high one, but their effectiveness depend on time.

From post mortem observations of MB0 samples, the energy absorbing mechanism associated to the liquid can only be speculated. At medium-high loading rates, it might act as crack bridges, more effective for high loading rates due to its low viscosity (high alkaline content). For the lowest strain rate, microstructural changes such as solution-precipitation and/or crystallization phenomena at the crack tip could take place leading to an increase of toughness.

5 Conclusions

The mechanical behaviour of two structural mullites with the same levels of impurities but different nature strongly depends on strain rate. This dependence shows different trends at room temperature and at high temperatures (1300°C).

Fracture behaviour at room temperature is determined by the distribution of the residual glassy phase:

(a) The glassy phase along grain boundaries leads to subcritical crack growth.
(b) When the glassy phase remains at triple points no subcritical crack growth takes place.

Fracture behaviour at high temperature is determined by the nature of the residual glassy phase which softens during testing:

(a) Decohesion of grains and liquid migration take place in mullite with higher alkali content (0·3%) due to the formation of low viscosity liquids.
(b) Grain boundary sliding is the main mechanism in mullite with low alkali content (< 0·1%) due to a higher viscosity of the liquids formed.

Acknowledgement

This work has been supported by CICYT, Project no. MAT 499-91.

References

1. Somiya, S. & Hirata, Y., Mullite Powder Technology and Applications in Japan. *Ceram. Bull.*, **70** (1991) 1624–32.
2. Sacks, M. D., Lee, H. W. & Pask, J. A., A Review of Powder Preparation Methods and Densification Procedures for Fabricating High Density Mullite. In *Mullite and Mullite Matrix Composites, Ceramic Transactions*, Vol. 6, The American Ceramic Society Inc., Ohio, 1990, pp. 167–213.
3. Baudín, C., Osendi, M. I. & Moya, J. S., Solid Solution of TiO_2 in Mullite. *J. Mater. Sci. Lett.*, **2** (1983) 185–7.
4. Baudín, C., Miranzo, P. & Osendi, M. I., High Temperature Mechanical Behaviour of $3Al_2O_3{:}2SiO_2$ Mullite Based Materials. In *Third Euro-Ceramics V-3*, Faenza Editrice Ibérica S.L, Spain, 1993, pp. 369–75.
5. Osborn, E. F. & Muan, A., plate no. 501, *Phase Diagrams for Ceramists*, The Am. Ceram. Soc. Inc., Ohio, USA, 1964.
6. Urbain, G., Cambier, F., Deletter, M. & Anseau, M. R., Viscosity of Silicate Melts. *Trans. J. Br. Ceram. Soc.*, **80** (1981) 139–41.
7. Fernandez Navarro, J. M., *El Vidrio*, Consejo Superior de Investigaciones Científicas, Spain, 1991, pp. 337–50.
8. Lessing, P. A., Gordon, R. S. & Mazdiyasny, K. S., Creep of Polycrystalline Mullite. *J. Am. Ceram. Soc.*, **58** (1975) 149.
9. Dokko, P. C., Pask, J. A. & Mazdiyasny, K. S., High Temperature Mechanical Properties of Mullite under Compression. *J. Am. Ceram. Soc.*, **60** (1977) 150–5.
10. Okamoto, Y., Fukudome, H., Hayashi, K. & Nishikawa, T., Creep Deformation of Polycrystalline Mullite. *J. Eur. Ceram. Soc.*, **6** (1990) 161–8.
11. Hynes, A. P. & Doremus, R. H., High Temperature Compressive Creep of Polycrystalline Mullite. *J. Am. Ceram. Soc.*, **74** (1991) 2469–75.
12. Ashizuka, M., Honda, T. & Kubota, Y., Effects of Grain size on Creep of Mullite Ceramics, *J. Ceram. Soc. Jpn. Int. Edition*, **99** (1991) 282–5.
13. Mah, T. I., Mazdiyasny, K. S., Mechanical Properties of Mullite. *J. Am. Cerm. Soc.*, **66** (1983) 699–703.
14. Yamade, Y., Kawaguchi, Y., Takeda, N. & Kishi, T., *J. Ceram. Soc. Jpn. Int. Edition*, **99** (1991) 452–7.
15. Kanzaki, S., Tabata, H., Sintering and Mechanical Properties of Stoichiometric Mullite. *J. Am. Ceram. Soc.*, **68** (1985) C6–7.
16. Ismail, M. G. M. U., Nakai, Z. & Somiya, S., Microstructure and Mechanical Properties of Mullite Prepared by Sol–Gel Method. *J. Am. Ceram. Soc.*, **70** (1987) C7–8.
17. Ohnishi, H., Maeda, K., Nakamura, T. & Kawanami, T., High Temperature Mechanical Properties of Mullite Ceramics, in Ref. 2, pp. 605–12.
18. Mizuno, M., Shiraishi, M. & Saito, H., Microstructure and Bending Strength of Highly Pure Mullite Ceramics, in Ref. 2 pp. 413–24.
19. Mizuno, M., Microstructure, Microchemistry and Flexural Strength of Mullite Ceramics. *J. Am. Ceram. Soc.*, **74** (1991) 3017–22.
20. Kaumazawa, T., Ohta, S., Nagaoka, T., Yasuoka, M. & Kanzaki, S., Influence of Powder Characteristics on Sinterability and Mechanical Properties of Silica–Alumina Ceramics (74 wt% Al_2O_3). *J. Ceram. Soc. Jpn. Int. Edition*, **99** (1991) 1191–6.
21. Bansal, G. K., Effect of Flaw Shape on Strength of Ceramics. *J. Am. Ceram. Soc.*, **59** (1976) 87–8.
22. Notis, M. R., Dravid, V. P. & Lyman, C. E., AEM and HRTEM Studies of the Eutectic System Zirconia-Mullite, in Ref. 2, pp. 528–39.
23. Torrecillas, R., Comportamiento Mecánico de Mullita y Mullita-Circona obtenida por sinterización reactiva, PhD Thesis. UNED, Madrid (Spain), 1990.
24. Cheeseman, C. R. & Groves, G. W., The Mechanism of Peak in Strength and Toughness at Elevated Temperatures in Alumina Containing a Glass Phase, *J. Mater. Sci.*, **20** (1985) 2614–22.
25. Rief, C. & Kromp, K., Fracture Toughness Testing. In *Mechanical Testing of Engineering Ceramics at High Temperatures*, Elsevier Applied Science, 1989, pp. 209–25.
26. Oda, I., Matui, M. & Sowa, T., High Temperature Fatigue Failure in Pressureless Sintered Silicon Nitride, In *Progress in Nitrogen Cermics*, Martinus Nijhoff Publisher, The Netherlands 1983, pp. 501–6.
27. Kriz, K., Fracture Behaviour of Hot Pressed Silicon Nitride between Room Temperature and 1400°C, in Ref. 26 pp. 523–8.